SCIENTIFIC REPORT

(12)

THE TWO-SLAB BURNING PROBLEM

By

R. R. Panyam and E. W. Price

Prepared for

OFFICE OF NAVAL RESEARCH
800 N. Quincy Street
Arlington, Virginia 22217

Under

Contract N00014-79-C-0764; NR 092-566

MARCH 1984

GEORGIA INSTITUTE OF TECHNOLOGY
A UNIT OF THE UNIVERSITY SYSTEM OF GEORGIA
SCHOOL OF AEROSPACE ENGINEERING
ATLANTA, GEORGIA 30332

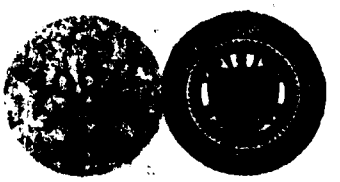

Unclassified

SECURITY CLASSIFICATION OF THIS PAGE *(When Data Entered)*

REPORT DOCUMENTATION PAGE		READ INSTRUCTIONS BEFORE COMPLETING FORM
1. REPORT NUMBER	2. GOVT ACCESSION NO. AD-A139 828	3. RECIPIENT'S CATALOG NUMBER
4. TITLE *(and Subtitle)* The Two-Slab Burning Problem		5. TYPE OF REPORT & PERIOD COVERED Scientific Report
		6. PERFORMING ORG. REPORT NUMBER
7. AUTHOR(s) Ramaprasad R. Panyam and Edward W. Price		8. CONTRACT OR GRANT NUMBER(s) ONR Contract No. N00014-79-C-0764
9. PERFORMING ORGANIZATION NAME AND ADDRESS School of Aerospace Engineering Georgia Institute of Technology Atlanta, Georgia 30332		10. PROGRAM ELEMENT, PROJECT, TASK AREA & WORK UNIT NUMBERS
11. CONTROLLING OFFICE NAME AND ADDRESS Mechanics Division, Office of Naval Research Department of the Navy, 800 N. Quincy Street Arlington, Virginia 22212		12. REPORT DATE March 1984
		13. NUMBER OF PAGES 43
14. MONITORING AGENCY NAME & ADDRESS*(if different from Controlling Office)*		15. SECURITY CLASS. *(of this report)* Unclassified
		15a. DECLASSIFICATION/DOWNGRADING SCHEDULE

16. DISTRIBUTION STATEMENT *(of this Report)*

Approved for public release; distribution unlimited.

17. DISTRIBUTION STATEMENT *(of the abstract entered in Block 20, if different from Report)*

Approved for public release; distribution unlimited.

18. SUPPLEMENTARY NOTES

19. KEY WORDS *(Continue on reverse side if necessary and identify by block number)*

COMBUSTION, SOLID PROPELLANT, ANALYSIS

20. ABSTRACT *(Continue on reverse side if necessary and identify by block number)*

Details of the propellant combustion zone microstructure were studied using the simpler configuration resulting from burning down the interface between contacting oxidizer and fuel slabs. Steady burning profiles and burning rates were determined experimentally for an ammonium perchlorate oxidizer and PMMA fuel. An iterative procedure was used to determine the heat source distribution in the gas phase that would produce the experimentally observed

DD FORM 1 JAN 73 1473 EDITION OF 1 NOV 65 IS OBSOLETE

Unclassified

SECURITY CLASSIFICATION OF THIS PAGE *(When Data Entered)*

protiles and burning rates. The procedure involved solution ot energy equations in the gas and solid, and the Navier-Stokes equations in the gas, and requiring that the experimentally-based boundary conditions in the solid and gas at the surtace be suitably matched. The results indicate the approximate dimensions and location ot the tlame zone, and details ot the thermal tield.

ACKNOWLEDGEMENT

This work was sponsored by the Mechanics Division of the Office of Naval Research. The technical monitor was Dr. R. S. Miller. This report is an abbreviated version of the Ph.D. thesis of the first author.

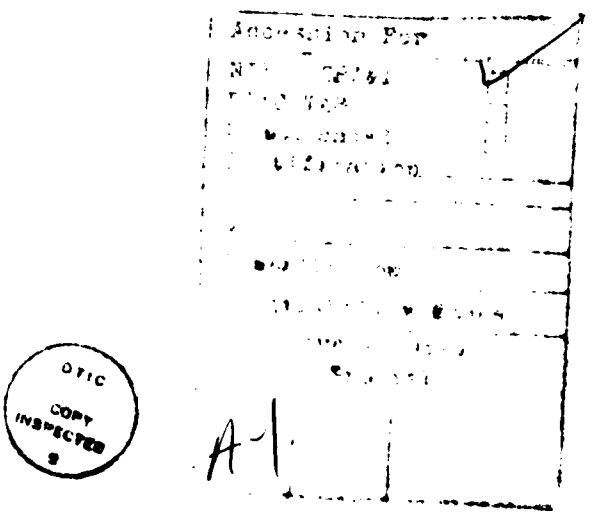

TABLE OF CONTENTS

INTRODUCTION

Composite solid propellants consist essentially of oxidizer particles of varying sizes interspersed in a binder matrix. The combustion of such a system is phenomenologically complex. A number of physico-chemical processes are known to occur. However, detailed knowledge of these processes is not currently available. Very significantly, many of these processes occur in a spatio-temporal extent which virtually forbids any meaningful experimental observation of the combustion mechanisms. In order to achieve any degree of predictive capability, analytical modeling of this system is necessary. A rigorous mathematical description of the combustion of composite propellants represents a formidable problem.

In an effort to circumvent some of the difficulties inherent in observation or analytical modeling of the combustion zone produced by the chaotic microstructure of a typical composite propellant, studies have been made of edge burning laminates. This configuration, called a "sandwich," consists of a layer of hydrocarbon fuel between two layers of oxidizer. This permits at least some fundamental aspects of composite propellant combustion to be reproduced within the framework of a simpler geometry that is easier to model analytically, and easier to observe experimentally than is possible with a propellant.

There is a large body of work on sandwich combustion. There are several experimental investigations (Ref. 1-14). These investigations include cinephotographic observations of burning sandwiches, optical/scanning electron microscope observations of quenched samples and schlieren observation of the gas phase structure. Several results are reported from burning rate measurements for different oxidizer-fuel combinations and laminate thicknesses

(Ref. 2,3,5-8,11). The combustion of sandwiches has been studied at several pressures.

While it is not clear that the microscopic flame is revealed in optical observations of combustion, its nature is suggested by visible density fluctuations above the flame (Ref. 6,10-12). High speed photography shows that this is related to a flickering or local intermittency along the flame sheet (Ref. 11). At pressures below the AP self-deflagration limit (~ 2 MPa), the flow above the flame is laminar. Systematic investigation of the surface profile of burning sandwiches has been made via the interrupted burn technique. The leading edge of regression is found to be in the oxidizer portion of the sample under several conditions (Ref. 4,8,10,13). A singular surface condition characterized as the "smooth band" has been observed in the oxidizer region close to the oxidizer-binder interfaces (Ref. 13,14). Sandwich deflagration limits have been found (Ref. 13). This is characterized as the binder thickness below which the sandwich does not burn at a given pressure.

There are several analytical investigations of sandwich combustion (Ref. 15-19). A comparison of the analytical and experimental investigations of sandwich combustion reveal certain gaps of analytical modeling to date. The analytical approaches have not succeeded in integrating into them even the widely recognized features of sandwich combustion. In particular, adequate use of the information on the surface profile geometry has not been made. A clear appreciation does not exist of the length scales involved in the dynamics of sandwich combustion. Most representations of the flame structure used in modeling are simple geometric entities which are unrealistic in view of the experimental evidence. Consequently, even the basic features of the microstructure of the flame complex remain unrecognized by theoreticians and

unmeasured by experimentalists. No quantitative theory exists that relates the structure of the flame complex and the details of the surface profile. Generally, simplistic representations are made of the fluid dynamical problem which is an inevitable concomitant of the thermal problem. It follows that no realistic estimates exist of the magnitude of the convective heat transfer in the problem. The present work attempts to address these issues.

It is easy to recognize that a model which incorporates all the features of sandwich combustion would be a very complex entity. The solution of such a system is held to be very difficult. The current model considers the simpler two-slab geometry. The philosophy of the current approach was to include as many of the experimentally observed features as deemed consistent with mathematical tractability. It was considered particularly important to include information on the surface profile, a quantity which can be observed with greater spatial resolution than any other relevant feature of the combustion zone (because of quench testing). The present approach is an inverse to the direct modeling of the combustion, in that the experimentally determined surface profile and sample burning rate are used as inputs to a calculation aimed at determining features of the flame complex. The analytical model was primarily motivated by the need to recover quantitative information about the gas flame microstructure. The specific objects of interest in the investigation are:

1) the characteristic length scales of the problem,

2) the nature of the flame structure, i.e., the magnitude and distribution of the heat release rate,

3) the role of fluid dynamics of the configuration, and

4) the sensitivity of the flame structure to a) changes in the surface profile, and b) the physical/ chemical properties that characterize the system.

Experimental work was also initiated, its object being the measurement of the surface profile of the oxidizer and the fuel and the interface burn rate.

MODEL DESCRIPTION

The model is concerned with the combustion at the interface of a semi-infinite slab of oxidizer and one of fuel. The shape of the typical burning surface profile is shown in Fig. 1. This figure is representative of the geometry considered in the model. The origin of the coordinate system is at the tip of the cavity and it rides the surface at the interface burning rate. The functions $y_{s1}(\hat{x})$ and $y_{s2}(\hat{x})$ describe the surfaces of the oxidizer and the fuel respectively, and $\bar{n}$ is the unit normal vector (positive) pointing outward into the gas phase.

The principal assumptions of the model are as follows:

1) The system achieves steady state. Under this condition, the geometry of the surface profile is not time dependent. There is experimental evidence to substantiate this claim (Ref. 6,10-12).

2) The model assumes that surface melts have negligible effect. This assumption restricts the interpretation of the results from the model to oxidizer-fuel systems that exhibit no or minimal melts under the conditions modeled.

3) The oxidizer and the fuel are assumed to pyrolyze at the surface in a manner describable by the classical Arrhenius rate law.

4) The oxidizer is assumed to be a non-monopropellant. The model would, however, be applicable to AP burning in this system below its deflagration limit. This restriction is only to ensure that the system burns in a geometry typified by the one in Fig. 1, used in the computational program.

5) All processes occurring in the system are two-dimensional. Several additional assumptions have been made to ensure computational simplicity.

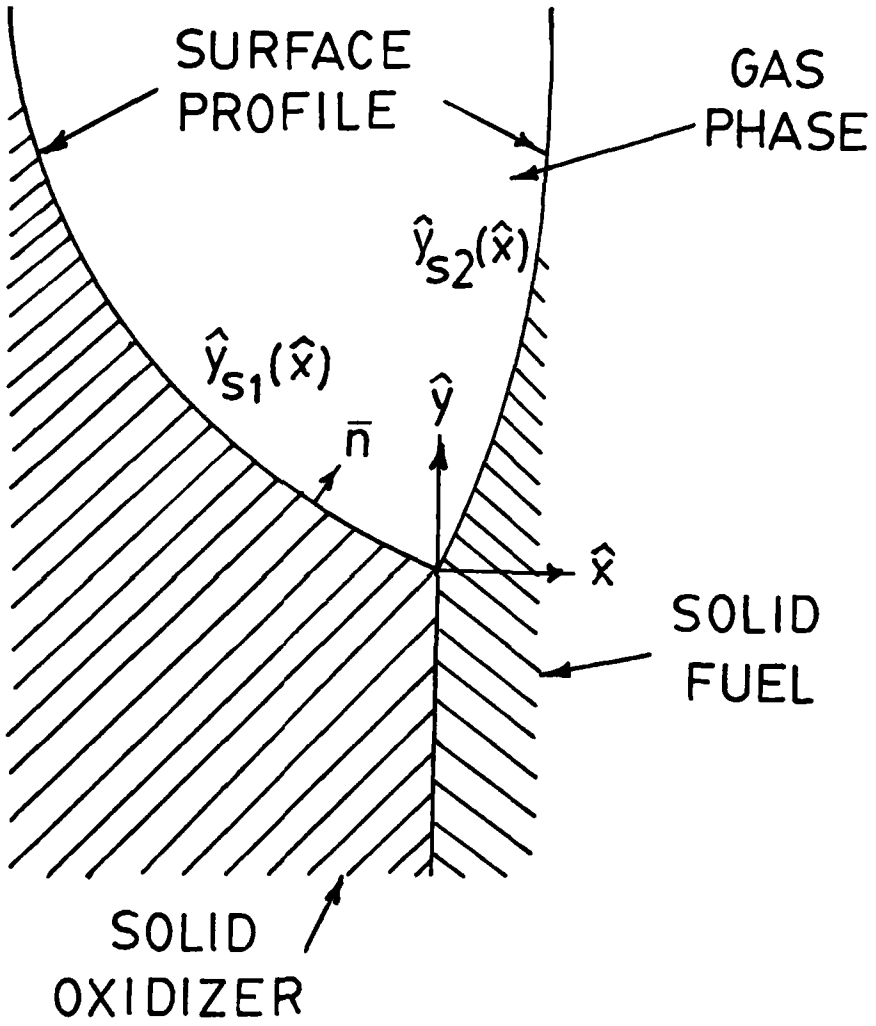

Figure 1. Geometry of the problem.

These are discussed in the context of their application. The equations and the boundary conditions which describe the system are discussed next.

Equation (1) is the two-dimensional energy equation for the gas phase.

$$\hat{\rho}_g \hat{C}_p \hat{u} \frac{\partial \hat{T}}{\partial \hat{x}} + \hat{\rho}_g \hat{C}_p \hat{v} \frac{\partial \hat{T}}{\partial \hat{y}}$$

$$- \hat{\lambda}_g \left(\frac{\partial^2 \hat{T}}{\partial \hat{x}^2} + \frac{\partial^2 \hat{T}}{\partial \hat{y}^2} \right) = \hat{F}(\hat{x}, \hat{y}) \qquad (1)$$

It is assumed that Le = 1 everywhere in the gas phase. Heat transfer is assumed to occur due to temperature gradients only. The variation of gas density with temperature is considered. The specific heat capacity and the thermal conductivity of the gas mixture (as well as those of the solid oxidizer and the solid fuel in Eq. (2) and (3)) are considered to be constants. The right hand side forcing function in Eq. (1) is the heat release rate per unit volume. It is the unknown which is sought. It may be pointed out that the description of the gas phase chemical reaction rate is implicitly lumped into this term. Individual species transport equations are not solved. It was thought that primary emphasis of this investigation should be directed toward energy distribution, rather than the chemistry of the process.

Equations (2) and (3) are the energy transport equations for the solid oxidizer and the fuel, respectively.

$$\hat{\rho}_1 \hat{r} \hat{C}_1 \frac{\partial \hat{T}}{\partial \hat{y}} - \hat{\lambda}_1 \left(\frac{\partial^2 \hat{T}}{\partial \hat{x}^2} + \frac{\partial^2 \hat{T}}{\partial \hat{y}^2} \right) = 0 \qquad (2)$$

$$\hat{\rho}_1 \hat{r}\, \hat{C}_2 \frac{\partial \hat{T}}{\partial \hat{y}} - \hat{\lambda}_2 \left(\frac{\partial^2 \hat{T}}{\partial \hat{x}^2} + \frac{\partial^2 \hat{T}}{\partial \hat{y}^2} \right) = 0 \qquad (3)$$

It is a requirement for steady state that there be no lateral velocities in the solids, and hence no term for convection in the $\hat{x}$ direction in Eq. (3).

Equation (4) is the statement of mass conservation for the two-dimensional flow.

$$\frac{\partial(\hat{\rho}\hat{u})}{\partial \hat{x}} + \frac{\partial(\hat{\rho}\hat{v})}{\partial \hat{y}} = 0 \qquad (4)$$

The variation of density is accounted for. The density varies not due to compressibility, but due to variation of temperature in the field. The flow is incompressible.

Equations (5) are the Navier-Stokes equations for the flow. It has been assumed that the flow is laminar, an assumption that is supported by the low Reynolds number and by experimental results for sandwiches burning at low pressures (Ref. 6,10-12).

$$\hat{\rho}\hat{u} \frac{\partial \hat{u}}{\partial \hat{x}} + \hat{\rho}\hat{v} \frac{\partial \hat{u}}{\partial \hat{y}}$$

$$= - \frac{\partial \hat{p}}{\partial \hat{x}} - \frac{\partial \hat{\tau}_{xx}}{\partial \hat{x}} - \frac{\partial \hat{\tau}_{xy}}{\partial \hat{y}}$$

$$\hat{\rho}\hat{u}\frac{\partial \hat{v}}{\partial \hat{x}} + \hat{\rho}\hat{v}\frac{\partial \hat{v}}{\partial \hat{y}}$$

$$= -\frac{\partial \hat{p}}{\partial \hat{y}} - \frac{\partial \hat{\tau}_{yy}}{\partial \hat{y}} - \frac{\partial \hat{\tau}_{xy}}{\partial \hat{x}} \qquad (5)$$

where,

$$\hat{\tau}_{xx} = 2/3\ \hat{\mu}\ \nabla\cdot\hat{\bar{v}} - 2\ \hat{\mu}\frac{\partial \hat{u}}{\partial \hat{x}}$$

$$\hat{\tau}_{yy} = 2/3\ \hat{\mu}\nabla\cdot\hat{\bar{v}} - 2\ \hat{\mu}\frac{\partial \hat{v}}{\partial \hat{y}}$$

$$\hat{\tau}_{xy} = -\hat{\mu}\left(\frac{\partial \hat{u}}{\partial \hat{y}} + \frac{\partial \hat{v}}{\partial \hat{x}}\right)$$

The velocity and the temperature fields are coupled by virtue of the variation of density with temperature. This has very important consequences for the entire model.

Equations (6) are the classical Arrhenius rate laws, which describe the pyrolysis taking place at the surface of the oxidizer and the fuel.

$$\hat{\rho}_i\hat{\bar{r}}\cdot\bar{n} = \hat{\rho}_i\hat{r}\,n_y = \hat{A}_i e^{-\hat{E}_i/(\hat{R}\,\hat{T}_{si})} \qquad i = 1,2 \qquad (6)$$

The constants in these equations are treated as known inputs to the model.

Equations (7) express the appropriate far field boundary conditions in the condensed phase.

$$\hat{T} \to \hat{T}_0 \text{ as } \hat{y} \to \infty \text{ for } -\infty < \hat{x} < \infty$$

$$\hat{T} \to \hat{T}_0 \text{ as } \hat{x} \to -\infty \text{ for } -\infty < \hat{y} < \infty$$

$$\hat{T} \to \hat{T}_0 \text{ as } \hat{x} \to \infty \text{ for } -\infty < \hat{y} < \infty$$

$$\hat{T} \to \hat{T}_0 \text{ as } \hat{y} \to -\infty \text{ for } -\infty < \hat{x} < \infty \qquad (7)$$

Equation (8) is a representation of the constancy of the heat flux on either side of the solid oxidizer - solid fuel interface.

$$\hat{\lambda}_1 \frac{\partial \hat{T}}{\partial \hat{x}} \Big|_{\hat{x}=0-} = \hat{\lambda}_2 \frac{\partial \hat{T}}{\partial \hat{x}} \Big|_{\hat{x}=0+} \text{ for } \hat{y} < 0 \qquad (8)$$

Equations (9) are the energy conservation laws at the interface between the gas and the solid phases.

$$\hat{\rho}_1 \hat{r} n_y \hat{h}_{s1} = \hat{\lambda}_g \left(n_x \frac{\partial \hat{T}}{\partial \hat{x}} + n_y \frac{\partial \hat{T}}{\partial \hat{y}} \right)_+$$

$$- \hat{\lambda}_1 \left(n_x \frac{\partial \hat{T}}{\partial \hat{x}} + n_y \frac{\partial \hat{T}}{\partial \hat{y}} \right)_- \quad \text{for } \hat{x} < 0 \text{; at the surface}$$

$$\hat{\rho}_2 \, \hat{r} \, n_y \, \hat{h}_{s2} = \hat{\lambda}_g \left(n_x \frac{\partial \hat{T}}{\partial \hat{x}} + n_y \frac{\partial \hat{T}}{\partial \hat{y}} \right)_+$$

$$- \hat{\lambda}_2 \left(n_x \frac{\partial \hat{T}}{\partial \hat{x}} + n_y \frac{\partial \hat{T}}{\partial \hat{y}} \right)_- \quad \text{for } \hat{x} > 0 \text{; at the surface} \tag{9}$$

It has been assumed that radiant transport of energy is not important. It has also been assumed that the kinetic energy at the interface is negligible. The surface processes that occur may either be endothermic or exothermic.

Equation (10) is a statement of mass conservation at the above interfaces.

$$\hat{\rho}_g \left(\hat{u}_w \, n_x + \hat{v}_w \, n_y \right) = \begin{cases} \hat{\rho}_1 \, \hat{r} \, n_y \text{ for } \hat{x} < 0 \\ \\ \hat{\rho}_2 \, \hat{r} \, n_y \text{ for } \hat{x} > 0 \end{cases} \tag{10}$$

Equations (11) describe the geometry of the problem.

$$\hat{h} \left(\hat{x}, \hat{y} \right) = 0 = \begin{cases} \hat{y} - \hat{y}_{s1} \left(\hat{x} \right) \text{ for } \hat{x} < 0 \\ \\ \hat{y} - \hat{y}_{s2} \left(\hat{x} \right) \text{ for } \hat{x} > 0 \end{cases} \tag{11}$$

$$\bar{n} = \frac{\nabla \hat{h}}{\| \nabla \hat{h} \|} = \left(n_x , n_y \right)$$

It may be noted that a non-symmetrical profile has been provided for.

APPROACH TO THE SOLUTION

The system of equations dealt with are elliptic partial differential equations. Equation (1) is nonlinear by virtue of the variation of gas phase density with temperature. Equations (5) are nonlinear. The domain on which the equations are valid is of rather complicated geometry. Based on these observations, it was decided to adopt a numerical approach.

At the outset, the surface profile geometry $\hat{h}(\hat{x},\hat{y})$ and the interface burn rate are specified. The pressure at which a steady state configuration characterized by the above is also known. The observation is made that the gas velocity vectors at the solid-gas interface are locally normal to the wall. This is a requirement of no slip flow. Using the above and Eq. (10), the velocity vector components at the wall are determined. If the temperature field is assumed, the density field can be determined. Upon a suitably defined closed domain (with appropriately defined bondary conditions) the Navier-Stokes equations can be solved to obtain the velocity field in the gas phase.

The specification of the interface burn rate and the surface profile results in the knowledge of the surface temperature distribution $\hat{T}_s(\hat{x},\hat{y})$, as seen from Eq. (6). This, in turn, permits the solution of the energy equations (2) and (3) in the solid phase. The boundary conditions (7) and (8) are used in this process. The condensed phase temperature field is thus computed. The computation of the temperature gradients at the surface in the solids is now possible.

We turn next to the gas phase energy equation, Eq. (1). The velocity field is known as a result of the solution of the Navier-Stokes equations. A plausible heat release rate distribution is assumed. The surface temperature distribution has already been determined. This, along with other boundary conditions, leads

to a solution of the temperature field in the gas phase. The density field can now be computed as well as the temperature gradients at the surface in the gas. Use of Eq. (9) is now invoked. The satisfaction of this condition to a specified accuracy is used as a matching condition. The process of solving Eq. (1) is repeated using improved estimates of $\hat{F}(\hat{x},\hat{y})$ until the required match is obtained.

It might be pointed out that a further overall iterative process involving the solutions to the gas momentum and energy equations is necessary. This is due to coupling between the two systems via the gas phase density. An appropriate overall convergence criterion may be defined for this process.

NUMERICAL TECHNIQUES

Navier-Stokes Equations

Experimental results point to the solid oxidizer and the solid fuel receding less and less rapidly farther away from the tip of the cavity. It has been assumed that the profile approximates a channel geometry far from the tip of the cavity. The geometry considered for the fluid problem is shown in Fig. 2. The walls BC and DE are no slip boundaries. BAE is the combustion driven inflow boundary. A Poiseuille boundary condition is initially used for the outflow boundary (though subsequent updates for this boundary are based on a "free" condition). The location at which this boundary condition is applied is decided by numerical experiments.

The boundary is transformed into a rectangle using the non-conformal transformation:

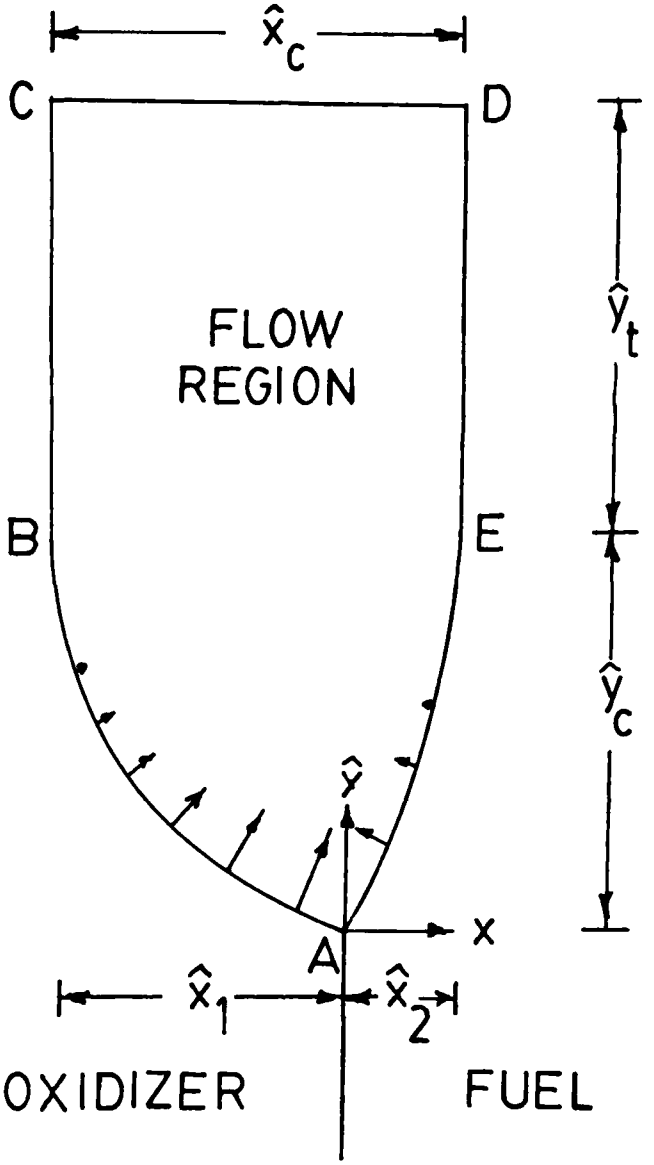

Figure 2. Fluid problem geometry.

$$\hat{\eta} = \hat{y} - \begin{cases} \hat{y}_{s1}\ (\hat{x}) & \text{for } \hat{x} > 0 \\ \\ \hat{y}_{s2}\ (\hat{x}) & \text{for } \hat{x} < 0 \end{cases} \tag{12}$$

The equations are non-dimensionalized in the conventional manner, and the problem is recast in vorticity-stream function variables. The solution can then be obtained for a known density distribution in the field. The nonlinear vorticity transport equation is solved by successive line under relaxation technique with linear extrapolation for the nonlinear terms. The boundary vorticities are updated by first order representations. The Poisson equation is solved by the successive line over relaxation method. A variable grid is provided in the $\hat{\eta}$ direction. The solutions to the vorticity transport equation and the Poisson equation are successively iterated within an overall iteration. The details of all computations in this work are reported elsewhere (Ref. 20). The solutions were obtained on a CDC 730/760 system. Typical computation times were on the order of 150 CPU secs. The streamlines were plotted by an auxiliary code.

Condensed Phase Energy Equations

The solution to the energy equation in the solid oxidizer and the solid fuel are obtained in tandem. The length scales are non-dimensionalized by $\hat{\alpha}_1/\hat{r}$ and the temperature by $\hat{T}_0$. The equations are then transformed using Eq. (12). The geometry and the boundary conditions for these equations are shown in Fig. 3. The numerical boundary conditions corresponding to Eqs. (7) are applied at finite distances whose locations are decided by numerical experiments. A special treatment of the code is necessary for the vertical interface. The solution is

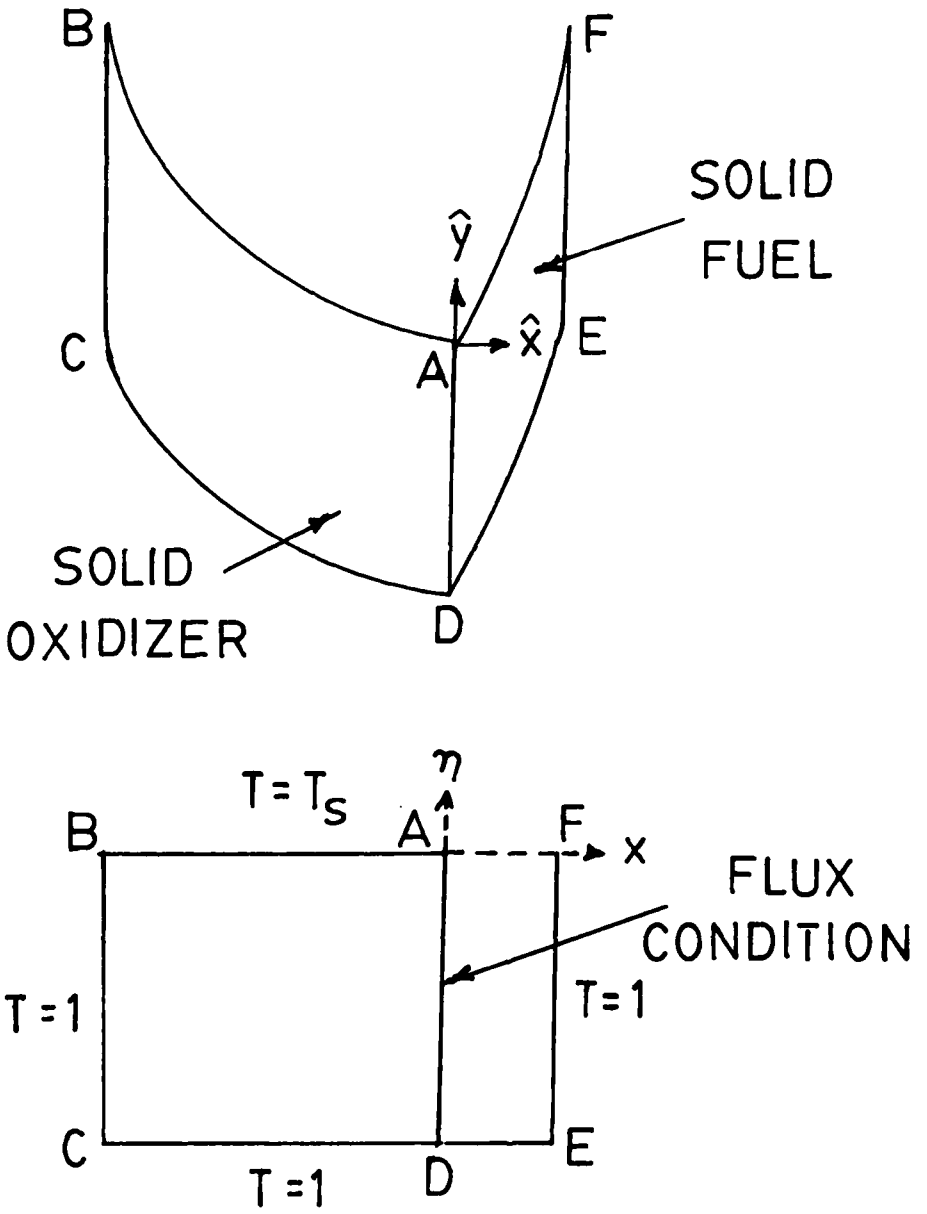

Figure 3. Geometry and boundary conditions for the condensed phase energy equation.

obtained by successive line over relaxation. The temperature field obtained is displayed as a plot of isotherms. Typical computational time on the CDC 760/730 system is about 40 CPU secs.

Gas Phase Energy Equation

The density in Eq. (1) is replaced by pressure and temperature by using the perfect gas law. The equation is then non-dimensionalized and transformed as before. The transformed domain is a rectangle as for the fluid problem. The equation can then be solved if the velocity field is known (from the solution of the Navier Stokes equations) and a heat release distribution is assumed. The nonlinear terms are linearized by extrapolating the values from previous iteration levels. The equation is solved by the successive line under relaxation method. The temperature field is displayed as a plot of isotherms. A typical solution takes about 100 CPU secs on the CDC 760/730 system.

MODULAR RESULTS

The baseline objective of this work is to obtain information on the gas phase combustion zone microstructure. This involves the solution of several equations in conjunction with each other within an overall iterative process. This procedure is not conducive to obtaining insight into the behavior of particular aspects of the system. It was therefore decided to work first with smaller, more easily comprehended parts. The condensed phase energy problem, the gas phase momentum problem and the gas phase energy problem constitute such modular entities. The object is, in each case, to delineate a general set of rules of behavior valid within a framework of constraints. It is acknowledged that care must be taken in interpreting these results in order that no more significance be

attributed to them than is warranted under the imposed constraints. Since the analytical work was initiated prior to the experimental part of this investigation, the surface profile and the interface burn rate from the investigation of Bakhman and Librovich (Ref. 7) corresponding to the combustion of KP-PMMA slab system at a pressure of 30 atm. was used for the following modular results.

Fluid Module

The code was initially run with constant density in the entire field. The velocity field so obtained was used in the computation of the solution of the gas phase energy equation along with an assumed nominal heat release distribution. From this the variable density field was computed. The solution to the momentum equations was again recomputed for the variable density case. The Re for this case was 58. Figure 4 shows the results obtained for the case with constant density as well as the one with variable density. It is a plot of streamlines. For the variable density case the flow preserves its two-dimensional character farther out. Also, the curvature of streamlines passing through the flame region is discernible. Apart from these qualitative changes, there are significant changes in the magnitudes of the velocities for the two cases. The coupling between the momentum and the energy equations is thus strong.

Condensed Phase Module

For representative values of thermophysical properties of KP and PMMA the solution obtained for the condensed phase energy equation is shown in Fig. 5. The temperatures in the figure are nondimensionalized. In the oxidizer the temperature gradients in the x-direction are considerably less than those in the y-direction. The isotherms, in general, tend to follow the surface profile. The

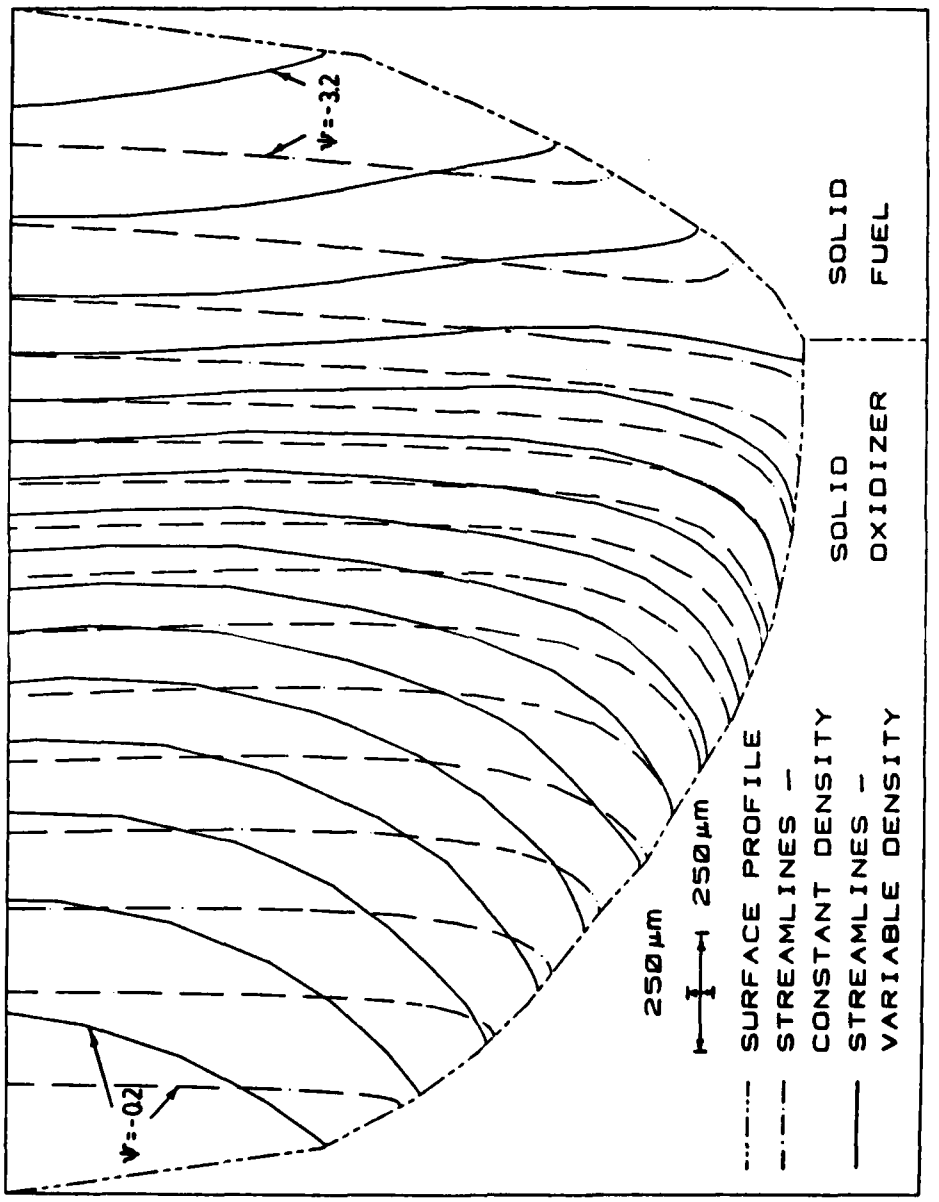

Figure 4. Streamline plot of the baseline fluid module solution.

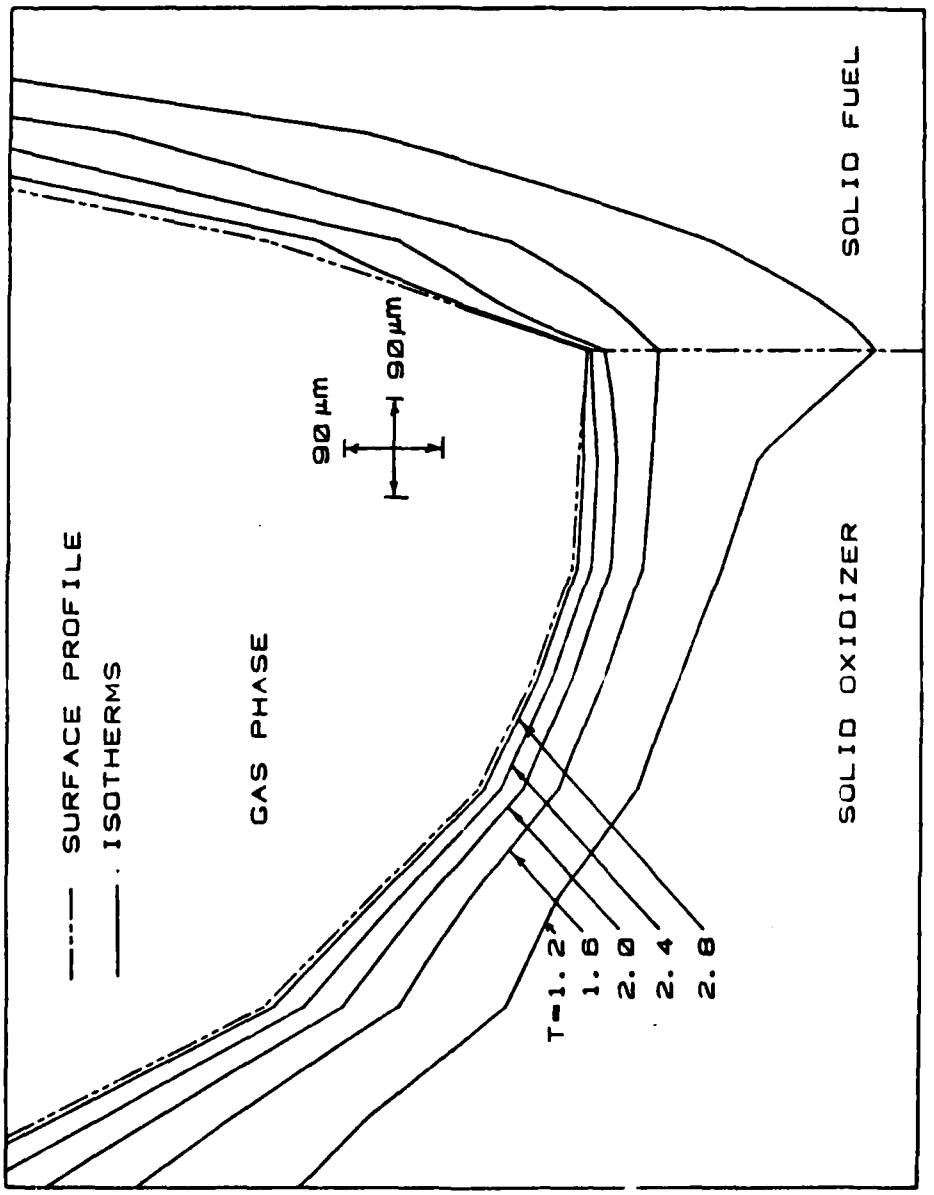

Figure 5. Baseline condensed phase isotherm plot.

direction of heat transfer at the vertical interface is toward the fuel at distances of the order of 50 μm from the tip of the cavity. At a distance of about 200 μm the vector, though very small in magnitude, is pointed toward the oxidizer. The effect of thermophysical properties of the oxidizer and the fuel has been studied in detail (Ref. 20). These affect the solution significantly in respect to the above considerations. The effect of the surface profile was also studied. It has been concluded that the slopes of the fuel and the oxidizer at the tip of the cavity significantly affect the magnitude and the direction of the heat flux vector at the vertical interface. The effect of pyrolysis kinetics on the temperature field enters via the surface temperature distribution. In general, the surface profile effects are more significant than the surface temperature distribution effects.

Gas Phase Module

Figure 6 shows the baseline result obtained for the gas phase energy equation with a heat release distribution assumed for a nominal match of the temperature gradients at the surface. It is a plot of isotherms. The results point to the bulk of the heat release occuring in a region less than about 500 μm from the tip of the cavity in the vertical direction. The lateral extent of the region is about 1500 μm. The maximum temperature occurs at about 60 μm from the surface.

It was found that values assumed for the specific heat and the thermal conductivity of the gases affect the solution significantly (Ref. 20). The effect of variation of the normalizing velocity on the solution is shown in Fig. 7. The figure dramatizes the effect in that the normalizing velocity is increased by a factor of 3 (cf Fig. 6, baseline case). The extent of the hot region increases and the maximum temperature drops. The role of convective heat transfer is very significant.

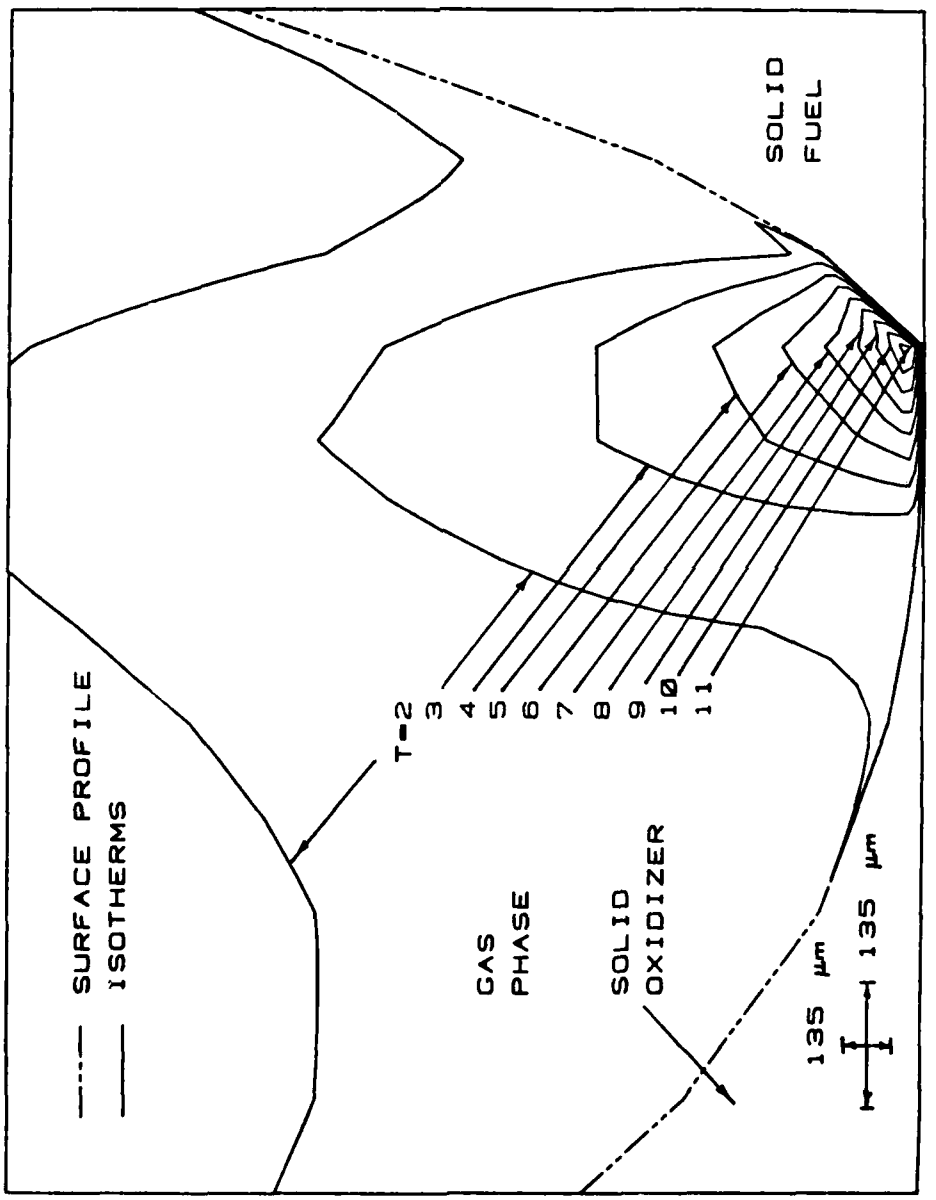

Figure 6. Baseline gas phase isotherm plot.

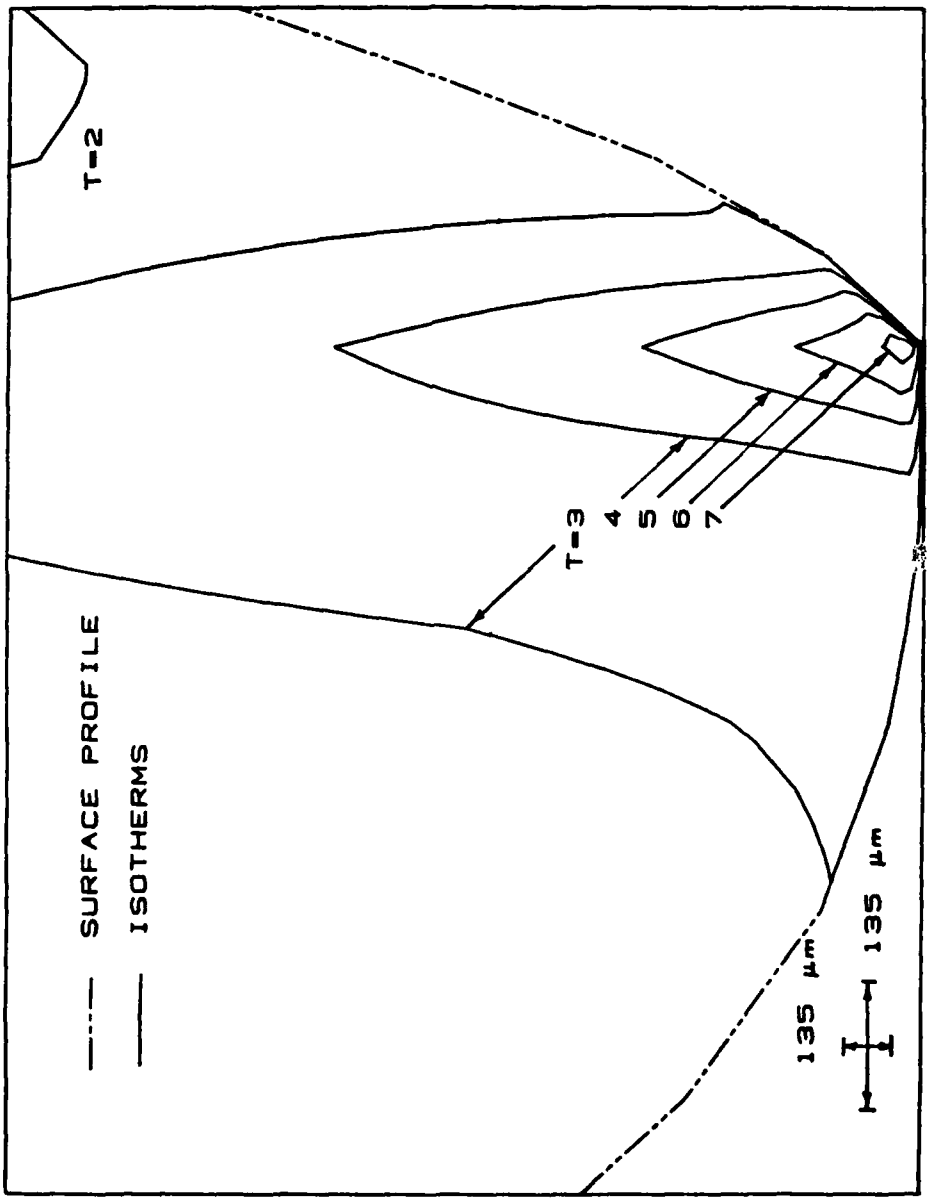

Figure 7. Effect of increase of normalizing convective velocity.

The effect of the magnitude and the distribution of the heat release was also studied. For instance, it was found that for volumetric heat release rates above about 6×10^5 cal/cm^3 sec, unrealistically high temperatures were obtained.

EXPERIMENTAL MEASUREMENTS

The surface profile and the interface burning rate have been obtained experimentally for use in the model. The burning sample is quenched and the surface profile determined by using an optical method. The burning rate was measured by using a cinephotographic technique. The details of these methods are described elsewhere (Ref. 20). The measurements were performed on the AP-PMMA slab system burned at pressures of 7.8 and 14.6 atm. Figure 8 shows the results of profile measurements for a test at 7.8 atm. The vertical dashed lines in the figure represent the conjecture regarding the location where the walls might become vertical. The data points which do not follow this trend are due to relaxation subsequent to softening and/or breaking at quench. The interface burning rate results are shown in Fig. 9. From the measurements of burning rates during the burning history of a sample, attainment of steady state was verified.

MODEL APPLICATION

In this section, the application of the entire model, as described in the section "Approach to the Solution," is considered. The consideration is based on the use of experimentally determined surface profiles and burn rates.

Let us consider the combustion of an AP-PMMA system at a pressure of 7.8 atm. Results were computed for the condensed phase energy equation, gas phase momentum equation and the gas phase energy equation based on input parameter

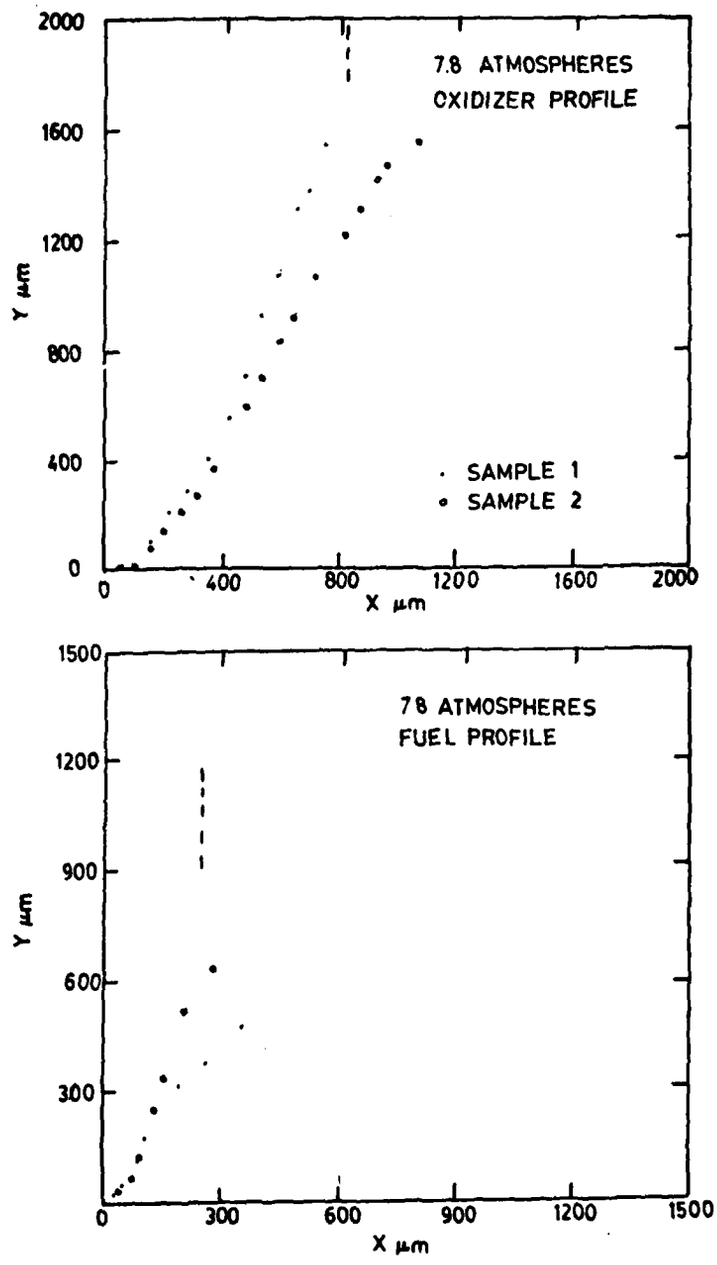

Figure 8. Experimentally determined surface profiles of fuel and oxidizer (7.8 atm.).

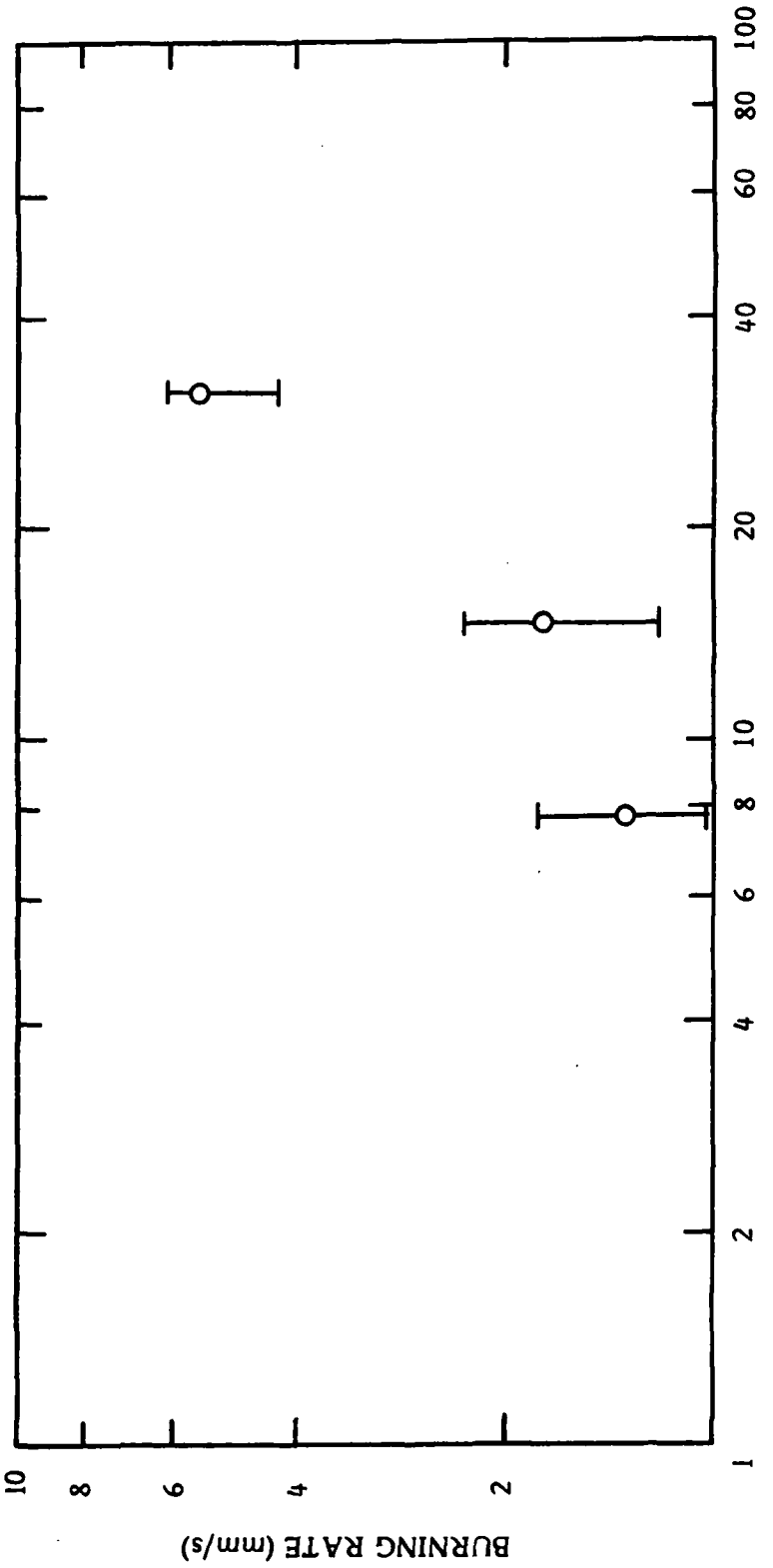

Figure 9. Measured interface burning rate for AP/PMMA slab system.

values in Tables 1, 2 and 3. The corresponding results are shown in Fig. 10, 11 and 12. The condensed phase results (Fig. 10) point to the heat being transferred from the oxidizer to the fuel at the vertical interface. Figure 11 shows the streamlines for the fluid solution. Figure 12 is a plot of isotherms for the gas phase. Figure 13 shows the heat release distribution which gave the above result. The maximum temperature in the gas is 2503°K and it occurs at about 1300 μm from the surface. All of the heat release has been assigned at locations below 5 mm from the surface. It may be pointed out that these results reflect the instance in which overall convergence has been obtained between the gas momentum and energy equations. The temperature gradients at the solid-gas interface have also been matched satisfactorily. (See Ref. 20 for details.) The total heat release rate has been computed from a thermodynamic point of view (Ref. 20). It has been found that about 20% of the heat release occurs at the surface. The method does not provide a unique solution, since it is based on an iterative procedure that requires only approximate matching of modular solutions to the conditions imposed by the input surface profile and burning rate. However, several other constraints are imposed (Ref. 20) to assure realistic results, and computer experiments have shown that the solution (including heat source distribution) is narrowly constrained by the procedure. Figure 14 shows the results for the gas phase energy equation from a similar series of computations for a pressure of 14.6 atm. The maximum temperature is 2711°K and it occurs at a distance of 700 μm from the surface.

CONCLUSIONS

A mathematical model has been developed for the combustion at the interface of an oxidizer-fuel slab system. The model is based on two-dimensional conservation equations and has been solved numerically. The model uses

Table 1. Values of input parameters for the condensed phase solution[20]
(pressure 7.8 atm.)

PHYSICAL CONSTANTS

OXIDIZER

ρ_1 = 1.95 gm/cm^3

c_1 = 0.3465 cal/gm ^oK

λ_1 = 0.0009 cal/cm sec ^oK

E_1 = 22000 cal/mole, $A_1 = 3. \times 10^5$ gm/cm^2 sec

FUEL

ρ_2 = 1.185 gm/cm^3

c_2 = 0.3 cal/gm ^oK

λ_2 = 0.0005 cal/cm sec ^oK

E_2 = 31000 cal/mole, $A_2 = 2.462 \times 10^7$

Slope of the oxidizer at the tip = 0.0
Slope of the fuel at the tip = 0.852
Interface burn rate = 0.133 cm/sec (experimental
Pressure = 7.8 atm.

Table 2. Values of input parameters for the fluid module solution[20]
(pressure 7.8 atm.)

PHYSICAL CONSTANTS

ρ_g = 0.00092 gm/cm^3 (pressure 7.8 atm.; temp 2782°K)

μ = 0.00075 gm/cm sec

V_0 = 80.2295 cm/sec

x_c = 1.094 mm

Re = 10.77

Table 3. Values of input parameters for the gas phase energy solution[20]
(pressure 7.8 atm.)

PHYSICAL CONSTANTS

λ = 0.0003 cal/cm sec ^{o}K

c_{pg} = 0.4272 cal/gm ^{o}K

ρ_g = 0.00092 gm/cm^3 (pressure 7.8 atm.; temp 2782^{o}K)

V_0 = 80.229 cm/sec p = 7.8 atm

T_0 = 298^{o}K r = 0.133 cm/sec

h_{s1} = -120 cal/gm h_{s2} = 314 cal/gm

T_f = 2782^{o}K M_g = 26.919

All condensed phase properties are as in Table 2.

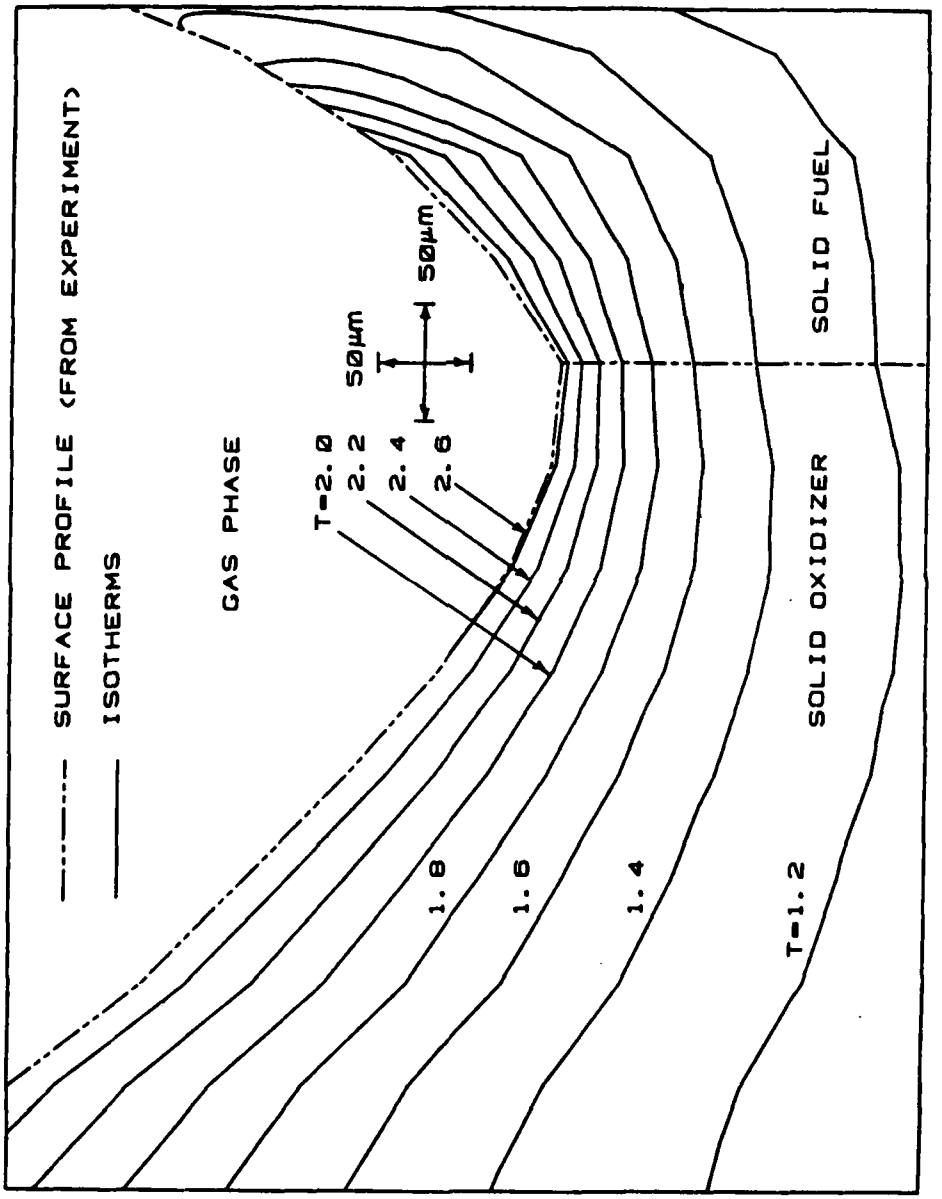

Figure 10. Condensed phase isotherm plot (pressure 7.8 atm.).

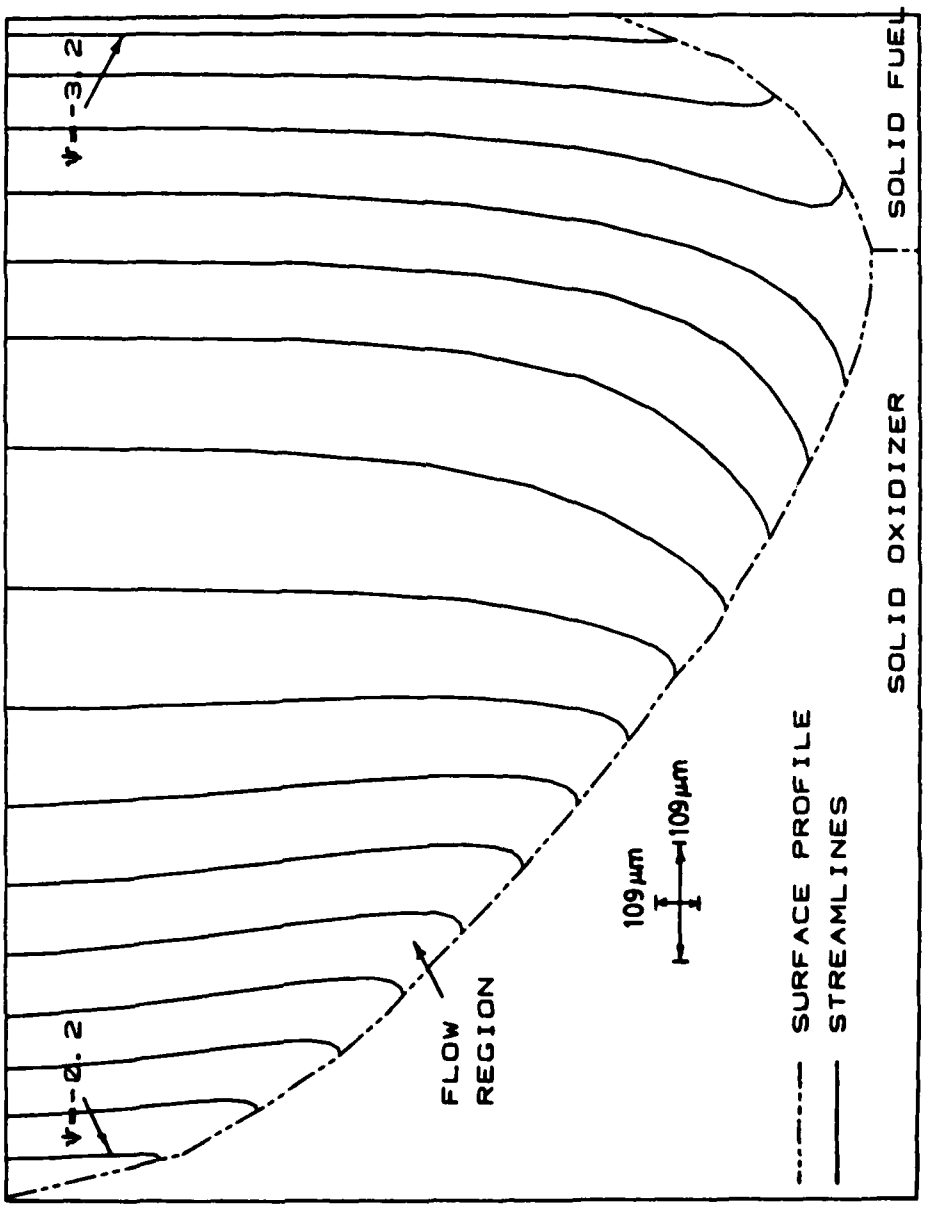

Figure 11. Streamline plot (pressure 7.8 atm.).

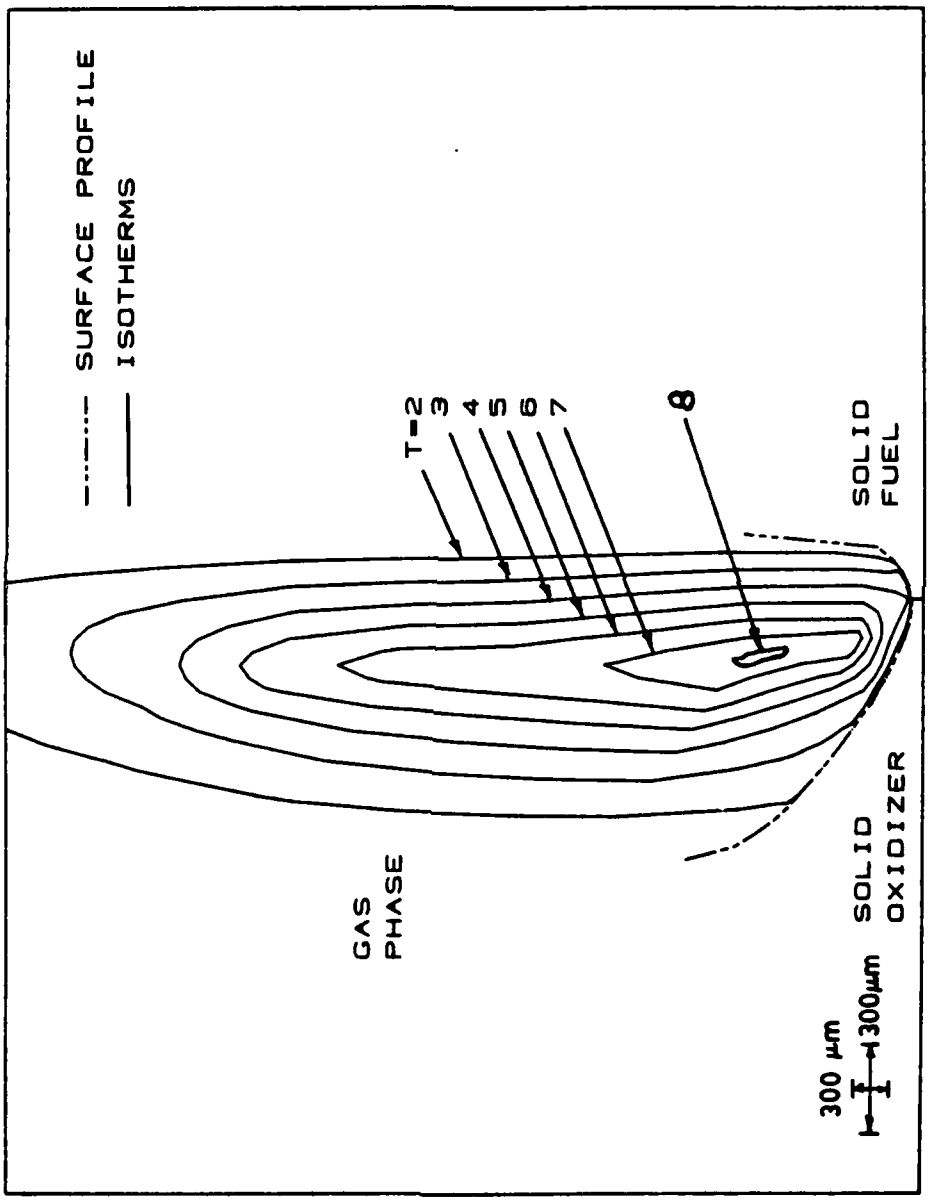

Figure 12. Gas phase isotherm plot (pressure 7.8 atm.).

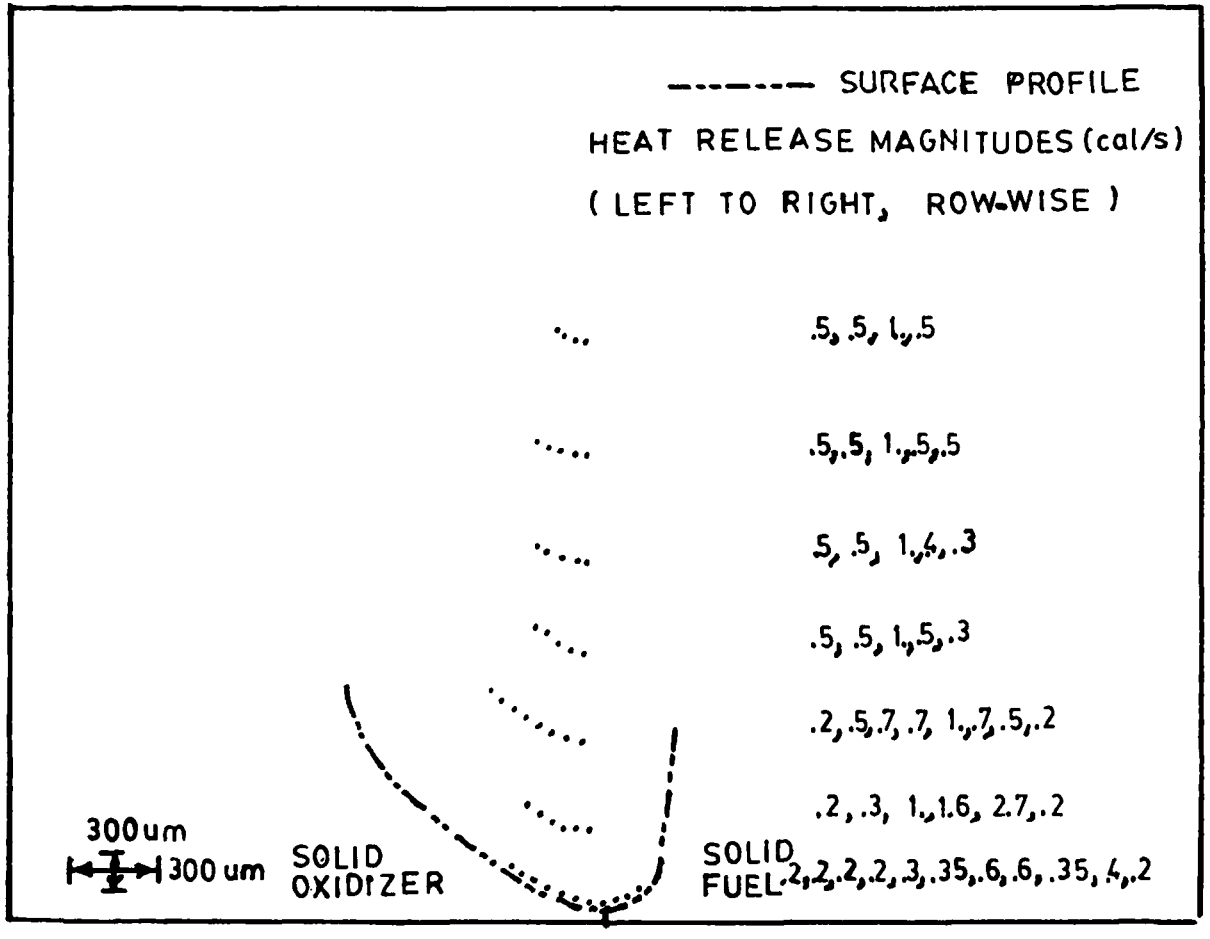

Figure 13. Gas phase heat release distribution (pressure 7.8 atm.).

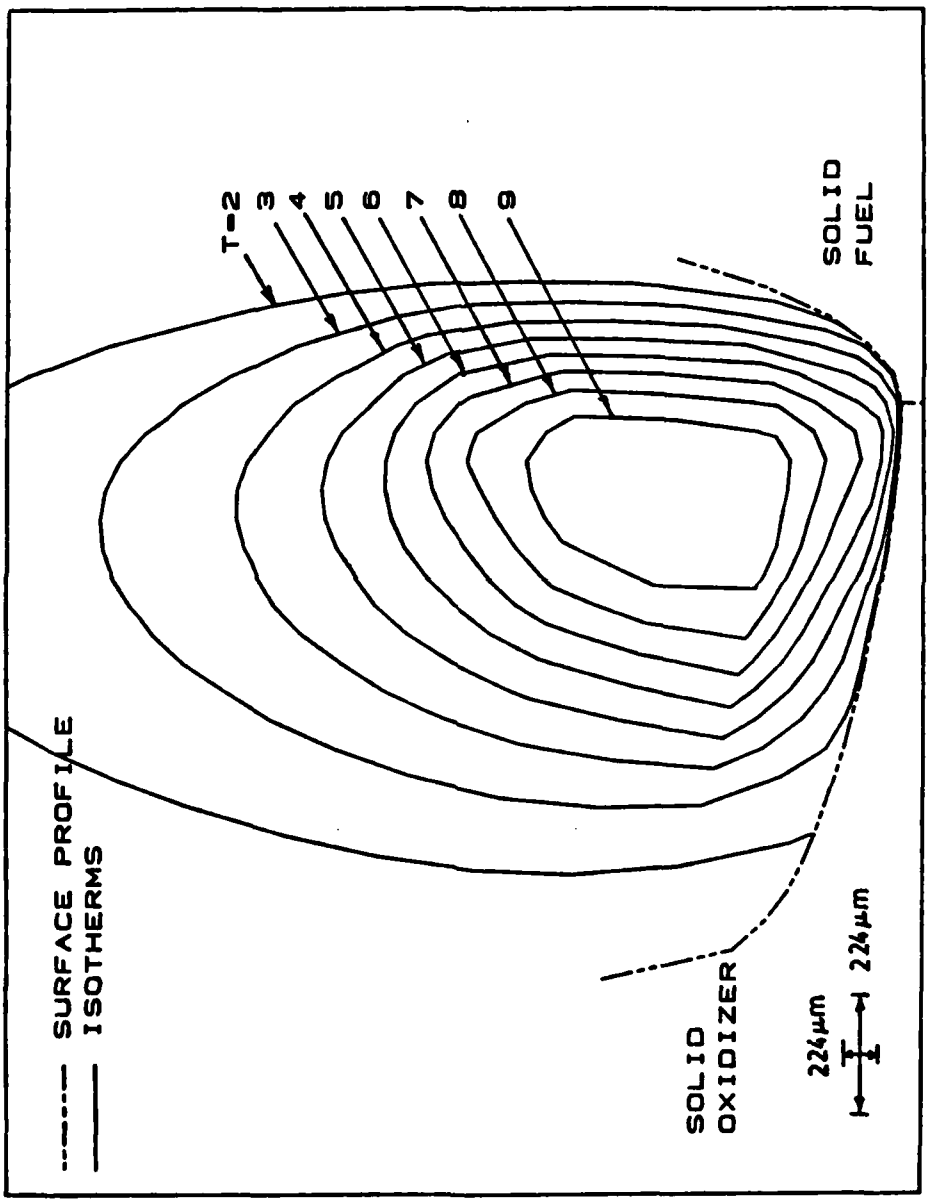

Figure 14. Gas phase isotherm plot (pressure 14.6 atm.).

experimentally determined burning surface profiles and burning rate as input, thereby avoiding the need for modeling the actual flame process.

The conclusions from the condensed phase energy solution are as follows:

1. The length scales over which significant temperature variations occur have been determined.
2. The heat transfer occurs from the oxidizer to the fuel at the vertical interface for the conditions studied.
3. The magnitudes of the thermal conductivities of the solids significantly affect the above conclusions.
4. In general, the shape of the surface profile affects the temperature field more significantly than the surface temperature distribution (i.e., the effect of surface decomposition kinetics is secondary). The results point to the importance of obtaining accurate experimental observations of the profile at the tip of the cavity.

Solutions have been obtained for the momentum equations with variable density inputs. The following observations are made in this context:

1. The inclusion of variable density leads to significant changes in the flow field (i.e., a constant-density assumption leads to significant error in calculation of the flow field).
2. The coupling between the momentum and energy equations is strong.
3. Satisfactory convergence has been obtained between these coupled solutions.

The gas phase energy equation has been solved. The solutions point to the following conclusions:

1. The solution is significantly affected by the specific heat and the thermal conductivity of the gas mixture.

2. The role of convective heat transfer is very significant in determining the gas phase flame structure (i.e., representation of heat flow in the gas by a conduction term alone leads to significant error in calculation of temperature fields and heat source distribution.

3. Realistic heat release rate distributions have been obtained.

4. It is believed that the magnitude and distribution of the heat release rate have been established within certain limits by the constraints imposed.

5. The surface heat release is of the order of 20% of the total heat released for the combustion of the system at 7.8 atm. (i.e., reasonable fit of condensed phase and gas phase solutions to observed surface profiles and burning rates could not be obtained without such heat release at the surface (even though the tests were at pressures below the self-deflagration limit of the AP.).

REFERENCES

1. Schultz, R., Green, L. and Penner, S. S., "Studies on the Decomposition Mechanism, Erosive Burning, Sonance and Resonance for Solid Composite Propellants," Combustion and Propulsion, Third AGARD Colloquium, Pergamon Press, New York, 1958, pp. 367-420.

2. Belayev, A. F. and Bakhman, N. N., "Theory of Burning of Powders and Solid Rocket Propellants," Fizika Goreniya i Vzryva, Vol. 2, No. 4, 1966, pp. 3-17.

3. Powling, J., "Experiments Relating to the Combustion of Ammonium Perchlorate-Based Propellants," 11th Symposium (International) on Combustion, The Combustion Institute, Pittsburgh, PA, 1967, pp. 447-456.

4. Hightower, J. D. and Price, E. W., "Experimental Studies Relating to the Combustion Mechanism of Composite Solid Propellants," Astronautica Acta, Vol. 14, 1968, pp. 11-21.

5. Nadaud, L., "Models Used at ONERA to Interpret Combustion Phenomena in Heterogeneous Solid Propellants," Combustion and Flame, Vol. 12, July 1968, pp. 177-195.

6. Ermolaev, A. F., Korotkov, A. I. and Frolov, Yu.V., "Laws of Combustion of a Solid Propellant Sandwich," Fizika Goreniya i Vzryva, Vol. 6, No. 3, July-Sept. 1970, pp. 277-285.

7. Bakhman, N. N. and Librovich, V. B., "Flame Propagation along Solid Fuel-Solid Oxidizer Interface," Combustion and Flame, Vol. 15, No. 9, October 1970, pp. 143-155.

8. Varney, A. M. and Strahle, W. C., "Experimental Combustion Studies of Two-Dimensional Ammonium Perchlorate-Binder Sandwiches," Combustion Science and Technology, Vol. 4, 1972, pp. 197-208.

9. Varney, A. M. and Strahle, W. C., "Thermal Decomposition Studies of Some Solid Propellant Binders," Combustion and Flame, Vol. 6, 1971, pp. 1-8.

10. Boggs, T. L. and Zurn, D. E., "The Deflagration of Ammonium Perchlorate-Polymeric Binder Sandwich Models," Combustion Science and Technology, Vol. 4, 1972, pp. 279-292.

11. Brown, W. E., Kennedy, J. R. and Netzer, D. W., "An Experimental Study of Ammonium Perchlorate-Binder Sandwich Combustion in Standard and High Acceleration Environments," Combustion Science and Technology, Vol. 6, 1972, pp. 211-222.

12. Murphy, J. L. and Netzer, D. W., "Ammonium Perchlorate and Ammonium Perchlorate-Binder Sandwich Combustion," AIAA Journal, Vol. 12, No. 1, Jan. 1974, pp. 13-14.

13. Price, E. W., Handley, J. C., Panyam, R. R., Sigman, R. K. and Ghosh, A., "Combustion of Ammonium Perchlorate-Polymer Sandwiches," AIAA Journal, Vol. 19, No. 3, March 1981, pp. 380-386.

14. Price, E. W., Panyam, R. R., Sambamurthi, J. K., and Sigman, R. K., "Combustion of Ammonium Perchlorate-Polymer Sandwiches," Annual Report to Office of Naval Research Contract, Georgia Institute of Technology, February 1983.

15. Nachbar, W., "A Theoretical Study of the Burning of a Solid Propellant Sandwich," Solid Propellant Rocket Research, Academic Press, New York, 1960, pp. 207-226.

16. Fenn, J. B., "A Phalanx Flame Model for the Combustion of Composite Solid Propellants," Combustion and Flame, Vol. 12, June 1968, pp. 201-216.

17. Strahle, W. C., "Solid Propellant Sandwich Deflagration Analysis," AIAA Journal, Vol. 13, No. 5, May 1975, pp. 640-696.

18. Guirao, C. and Williams, F. A., "A Model for Ammonium Perchlorate Deflagration between 20 and 100 Atmospheres," AIAA Journal, Vol. 9, July 1971, pp. 1345-1356.

19. Anikeev, V. I., Korobeinichev, O. P. and Schemev, A. S., "Combustion of Heterogeneous Systems with Constituents Capable of Evaporating and Reacting in the Condensed and the Gas Phases," Fizika Goreniya i Vzryva, Vol. 15, No. 2, March-April 1979, pp. 179-186.

20. Panyam, R. R., "Combustion at the Interface of an Oxidizer-Fuel Slab System," Ph.D. Thesis, Georgia Institute of Technology, June 1983.

NOMENCLATURE

A	pre-exponential factor in Arrhenius rate law (gm/cm^2 sec) *
C	specific heat of solid phase (cal/gm^oK)
C_p	specific heat of gas mixture (cal/gm^oK)
D	diffusion coefficient (cm^2/sec)
E	activation energy (cal/mole)
F	volumetric heat release rate (cal/cm^3 sec)
h	heat of gasification (cal/gm)
H	heat of formation (cal/mole)
Le	Lewis number, $\lambda / \rho D C_p$
M	molecular weight
$\bar{n}$	unit normal vector at surface
n_x, n_y	x and y components of $\bar{n}$
p	pressure (atm., other)
r	interface burn rate (cm/sec)
Re	Reynolds number, $x v \rho / \mu$

---

* units in parentheses apply to corresponding dimensional quantities.

T	temperature (^{o}K)
u	velocity in the x-direction (cm/sec)
v	velocity in the y-direction (cm/sec)
V_0	normalizing velocity (cm/sec)
V_n	surface normal velocity (cm/sec)
x	abcissa
y	ordinate
z	$\sqrt{1 + y_s'^2}$
α	thermal diffusivity (cm^2/sec)
η	transformed y co-ordinate
λ	thermal conductivity ($cal/cm\ sec\ ^{o}K$)
μ	viscosity of gas mixture (gm/cm sec)
ρ	density (gm/cm^3)
τ	shear stress, normal stress
ψ	stream function

Subscripts

c	channel
g	gas mixture

n	normal to the surface
s	surface
t	transition
w	wall (surface)
x	x-direction
y	y-direction
0	conditions at infinity
1	oxidizer
2	fuel

Superscripts

^	dimensional quantity
′	d/dx
″	d^2/dx^2
—	vector

DISTRIBUTION LIST

	No. Copies
Assistant Secretary of the Navy (R, E, and S) Room 5E 731 Pentagon Washington, DC 20350 Attn: Dr. L. V. Schmidt	1
Scientific Advisor Commandant of the Marine Corps Code RD-1 Washington, DC 20380 Attn: Dr. A. L. Slafkosky	1
Office of Naval Research Mechanics Division Code 432 Arlington, VA 22217 Attn: Dr. A. D. Wood	1
Office of Naval Research Mechanics Division Code 432 Arlington, VA 22217 Attn: Dr. Richard S. Miller	10
Office of Naval Research Code 260 Arlington, VA 22217 Attn: Mr. David Siegel	1
Office of Naval Research Western Office 1030 East Green Street Pasadena, CA 91106 Attn: Dr. R. J. Marcus	1
Office of Naval Research East Central Regional Office 666 Summer Street, Bldg. 114-D Boston, MA 02210 Attn: Dr. Larry Peebles	1
Office of Naval Research San Francisco Area Office One Hallidie Plaza, Suite 601 San Francisco, CA 94102 Attn: Dr. Phillip A. Miller	1
Aerojet Solid Propulsion Company P. O. Box 13400, Bldg. 2019/Dept. 4350 Sacramento, CA 95813 Attn: Mr. Michael J. Ditore	1
Aerojet Strategic Propulsion Co. P. O. Box 15699C Sacramento, CA 95813 Attn: Dr. R. L. Lou	1
Aerospace Corporation P. O. Box 92957 Los Angeles, CA 90045 Attn: Ellis M. Landsbaum	1
U. S. Air Force Academy FJSRL/NC USAF Academy, CO 80840 Attn: Dr. John S. Wilkes, Jr.	1
AFATL Code DLDL Eglin AFB, FL 32542 Attn: Mr. Otto K . Heiney	1
Air Force Office of Scientific Research Directorate of Aerospace Sciences Bolling Air Force Base Washington, DC 20332 Attn: Dr. L. H. Caveny	1
Air Force Office of Scientific Research Directorate of Chemical Sciences Bolling Air Force Base Washington, DC 20332 Attn: Mr. Donald L. Ball	1
AFRPL Code PACC Edwards AFB, CA 93523 Attn: Mr. Wayne Roe Mr. J. Levine	2
AFRPL Code MKP/MS24 Edwards AFB, CA 93523 Attn: Mr. R. Geisler	1
AFRPL Code CA Edwards AFB, CA 93523 Attn: Dr. R. R. Weiss	1
Anal-Syn Lab Inc. P. O. Box 547 Paoli, PA 19301 Attn: Dr. V. J. Keenan	1
Army Ballistic Missile Defense Command BMDSC/HEDS P. O. Box 1500 Redstone Arsenal, AL 35807 Attn: Ms. R. Buckalew	1
Army Ballistic Research Labs ARRADCOM Code DRDAR-BLI Aberdeen Proving Ground, MD 21005 Attn: Mr. J. M. Frankle Dr. Ingo W. May Mr. L. A. Watermeier	3
Army Ballistic Research Labs ARRADCOM Code DRDAR-BLP Aberdeen Proving Ground, MD 21005 Attn: Dr. A. W. Barrows	1
HQ US Army Material Development Readiness Command Code DRCDE-DW 5011 Eisenhower Avenue Room 8N42 Alexandria, VA 22333 Attn: Mr. S. R. Matos	1
Army Missile Command Code DRSMI-R Redstone Arsenal, AL 35898 Attn: Dr. R. G. Rhoades	1
Army Missile Command Code DRSMI-RKL Redstone Arsenal, Al 35898 Attn: Dr. W. W. Wharton	1
Army Research & Development Command ARRADCOM Code LCWSL Dover, NJ 07802	1
Army Research & Development Command ARRADCOM Code DRDAR-SCA-PE Dover, NJ 07802 Attn: Mr. L. Stiefel	1
U. S. Army Research Office Chemical & Biological Sciences Div. P. O. Box 12211 Research Triangle Park, NC 27709	1
Atlantic Research Corp. 4390 Cherokee Ave. Alexandria, VA 22314 Attn: Dr. C. B. Henderson Dr. Merill K. King	2
Atlantic Research Corp Pine Ridge Plant 7511 Wellington Rd. Gainesville, VA 22065 Attn: Mr. R. H. W. Waesche	1
Brigham Young University Provo, UT 84601 Attn: Dr. Merrill W. Beckstead	1
British Embassy Munitions Directorate Propellants and Explosives Defence Equipment Staff 3100 Massachusetts Ave. Washington, DC 20008 Attn: Dr. T. Sinden	1
California Institute of Tech. Graduate Aeronautical Lab Pasadena, CA 91125 Attn: Prof. W. G. Knauss	1
California Institute of Tech. Dept. of Chemical Engineering Pasadena, CA 91125 Attn: Prof. N. W. Tschoegl	1
California Institute of Tech. 204 Karman Lab 1201 E. California St. Pasadena, CA 91109 Attn: Fred E. C. Culick	1

DISTRIBUTION LIST

	No. Copies
Naval Materiel Command Strategic Systems Project Office Propulsion Unit Code SP 2731 Department of the Navy Washington, DC 20376	1
Naval Materiel Command Strategic Systems Project Office Department of the Navy Room 1048 Washington, DC 20376 Attn: Mr. E. L. Throckmorton	1
Naval Ocean Systems Center San Diego, CA 92152 Attn: Mr. Joe McCartney	1
Naval Ocean Systems Center Marine Sciences Division San Diego, CA 91232 Attn: Dr. S. Yamamoto	1
Naval Ordnance Station PM4 Indian Head, MD 20640 Attn: Mr. C. L. Adams	1
Naval Ordnance Station Code 5253 Indian Head, MD 20640 Attn: Mr. S. Mitchell	1
Naval Ordnance Station Indian Head, MD 20640 Attn: Mr. Peter L. Stang	1
Naval Postgraduate School Dean of Research Monterey, CA 93940 Attn: Dr. William Tolles	1
Naval Postgraduate School Physics & Chemistry Dept. Monterey, CA 93940 Attn: Prof. Richard A. Reinhardt	1
Naval Postgraduate School Department of Aeronautics Monterey, CA 93940 Attn: Mr. David W. Netzer	1
Naval Research Lab. Code 4040 Washington, DC 20375 Attn: Dr. Elaine Oran	1
Naval Research Lab. Code 6100 Washington, DC 20375	1
Naval Research Lab. Code 6510 Washington, DC 20375 Attn: Dr. J. Schnur	1
Naval Sea Systems Command Code SEA 64E Washington, DC 20362 Attn: Mr. R. Beauregard	1
Naval Sea Systems Command Code 62R3 Washington, DC 20362 Attn: Mr. G. Edwards	1
Naval Sea Systems Command NAV SEA 62R22 Crystal Plaza, Bldg. 6, Rm 806 Washington, DC 20362 Attn: Mr. Robert F. Cassel	1
Naval Sea Systems Command Code 62R2 Washington, DC 20362 Attn: Mr. C. M. Christensen	1
Naval Ship Engineering Center Materials Branch Philadelphia, PA 19112 Attn: Mr. John Boyle	1
Naval Ship Research & Development Center Applied Chemistry Division Annapolis, MD 21401 Attn: Dr. G. Bosmajian	1
Naval Surface Weapons Center Commander Silver Spring, MD 20910 Attn: Mr. G. B. Wilmot	4
Naval Surface Weapons Center Code RO4 White Oak Laboratory Silver Spring, MD 20910 Attn: Dr. D. J. Pastine	1
Naval Surface Weapons Center Code R10 White Oak Laboratory Silver Spring, MD 20910 Attn: Dr. S. J. Jacobs	1
Naval Surface Weapons Center Code R11 White Oak Laboratory Silver Spring, MD 20910 Attn: Dr. H. G. Adolph Dr. T. Hall Dr. M. J. Kamlet Dr. K. F. Mueller	4
Naval Surface Weapons Center Code R13 White Oak Laboratory Silver Spring, MD 20910 Attn: Dr. E. Zimmet Dr. R. Bernecker	2
Naval Surface Weapons Center Code R16 Indian Head, MD 20640 Attn: Dr. T. D. Austin	1
Naval Surface Weapons Center Code R101 Indian Head, MD 20640 Attn: Mr. G. L. Mackenzie	1
Naval Surface Weapons Center Code R121 White Oak Laboratory Silver Spring, MD 20910 Attn: Mr. M. Stosz	1
Naval Surface Weapons Center Code R122 White Oak Laboratory Silver Spring, MD 20910 Attn: Mr. L. Roslund	1
Office of Naval Technology Chief MAT Code 0716 Washington, DC 20360 Attn: Dr. A. Faulstich	1
Office of Naval Technology Chief of Naval Material MAT Code 0712 Washington, DC 20360 Attn: LCDR J. Walker	1
Naval Underwater Systems Center Energy Conversion Dept. Code 5B331 Newport, RI 02840 Attn: Mr. Robert S. Lazar	1
Naval Weapons Center Code 385 China Lake, CA 93555 Attn: Dr. A. Amster Dr. A. Nielsen	2
Naval Weapons Center Code 389 China Lake, CA 93555 Attn: Mr. T. L. Boggs Dr. R. L. Derr Dr. R. Reed, Jr.	3
Naval Weapons Center Code 3205 China Lake, CA 93555 Attn: Mr. Lee N. Gilbert Dr. L. Smith Dr. C. Thelen	3
Naval Weapons Center Code 3272 China Lake, CA 93555 Attn: Mr. R. McCarten	1
Naval Weapons Center Code 3858 China Lake, CA 93555 Attn: Dr. E. Martin	1

DISTRIBUTION LIST

	No. Copies
Naval Weapons Support Center Code 5042 Crane, IN 47522 Attn: Dr. B. Douda	1
Northwestern University Dept. of Civil Engineering Evanston, IL 60201 Attn: Prof. J. D. Achenbach	1
Pennsylvania State University Dept. of Mechanical Engineering University Park, PA 16802 Attn: Prof. Kenneth Kuo	1
Princeton Combustion Research Laboratories, Inc. 1041 U. S. Highway One North Princeton, NJ 08540 Attn: Dr. Martin Summerfield Dr. J. Ben Raven	2
Princeton University School of Engineering and Applied Sciences Dept. of Mech. Eng. & Aero. Eng. The Engineering Quadrangle Princeton, NJ 08544 Attn: Dr. Forman A. Williams	1
Purdue University School of Mechanical Engineering TSPC Chaffee Hall West Lafayette, IN 47906 Attn: Mr. John R. Osborn	1
Rockwell International Corp. Rocketdyne Division BA08 6633 Canoga Ave. Canoga Park, CA 91304 Attn: Mr. Joseph E. Flanagan	1
Rohm and Haas Company Huntsville, AL 35801 Attn: Dr. H. Shuey Mr. W. Stone	2
Sandia Laboratories Division 2513 P. O. Box 5800 Albuquerque, NM 87185 Attn: Dr. S. Sheffield	1
Space Sciences, Inc. 135 Maple Avenue Monrovia, CA 91016 Attn: Dr. M. Farber	1
Southwest Research Institute Institute Scientist P. O. Drawer 28510 San Antonio, TX 78228 Attn: Mr. William H. McLain	1
Texas A & M University Dept. of Civil Engineering College Station, TX 77843 Attn: Prof. Richard A. Schapery	1
United Technologies Corp. Chemical Systems Division P. O. Box 358 Sunnyvale, CA 94088 Attn: Dr. Robert S. Brown Dr. C. M. Frey Dr. R. W. Hermsen	3
University of Akron Institute of Polymer Science Akron, OH 44325 Attn: Prof. Alan N. Gent	1
University of California Berkeley, CA 94720 Attn: Prof. A. G. Evans	1
University of California Dept. of Chemistry 405 Hilgard Ave. Los Angeles, CA 90024 Attn: Prof. M. D. Nicol	1
University of Delaware Department of Chemistry Newark, DE 19711 Attn: Dr. T. C. Brill	1
University of Illinois AE Dept. Transportation Building, Room 105 Urbana, IL 61801 Attn: Dr. Herman Krier	1
University of Maryland Dept. of Mechanical Engineering College Park, MD 20742 Attn: Prof. R. W. Armstrong	1
University of Southern California Mechanical Engineering Dept. OHE 200 Los Angeles, CA 90007 Attn. Dr. M. Gerstein	1
University of Utah Salt Lake City, UT 84112 Attn: Dr. G. A. Flandro	1
University of Utah Dept. of Mech. & Ind. Eng. MEB 3008 Salt Lake City, UT 84112 Attn: Dr. Stephen Swanson	1
University of Waterloo Dept. of Mechanical Engineering Waterloo, Ontario CANADA Attn: Dr. Clarke E. Hermance	1
Washington State University Dept. of Physics Pullman, WA 99163 Attn: Prof. G. D. Duvall Prof. T. Dickinson	2
Whittaker Corporation Bermite Division 22116 W. Soledad Canyon Road Saugus, CA 90024 Attn: Mr. L. Bloom	1